Int. J. Electrochem. Sci., 16 **(2021)** Article ID: 21097, doi: 10.20964/2021.09.34

International Journal of
ELECTROCHEMICAL
SCIENCE
www.electrochemsci.org

A Novel Fading Memory Recursive Least Square Method (FMLS) for Accurate State of Charge Estimation of Lithium-ion Batteries Combined with Improved Second Order PNGV M odeling

Donglei Liu, Yongcun Fan[*]*, Shunli Wang*[*]*, Lili Xia, Jingsong Qiu, Etse Dablu Bobobee*

School of Information Engineering, Southwest University of Science and Technology, Mianyang 621010, China
[*]E-mail:8121064@qq.com, 497420789@qq.com.

Received: 27 May 2021 / *Accepted:* 9 July 2021 / *Published:* 10 August 2021

As the main energy storage element and power source of electric vehicles, the accurate estimation of the state of charge (SOC) of lithium-ion batteries is very important for the battery management system of electric vehicles, as well as for the driving range and safety. To accurately describe the characteristics of the lithium-ion battery, an improved PNGV model was formed by connecting an RC circuit based on the traditional PNGV lithium battery equivalent model. Considering the aging characteristics of lithium batteries in use, the recursive least square method (FMRLS) with fading memory was adopted to identify parameters to meet the requirements of estimation accuracy, and the Extended Kalman Filter (EKF) algorithm was used to estimate SOC. The accuracy of MAE, MAPE and RMSE was improved by 9.21%, 4.85% and 9.38% respectively under DST condition. The improvement was 34.35%, 36.59% and 31.97%, respectively, Under BBDST condition.

Keywords: lithium-ion batteries; state of charge estimation; electrical equivalent circuit model; FMRLS; Extended Kalman filter

1. INTRODUCTION

The lithium-ion battery has the advantages of long life, good stability, moderate cost, high energy density, environmental protection, and no pollution. Since it was first commercialized by Sony in 1991, it has been widely used in portable electronic products. The development of new energy[1] and the demand for large-scale energy storage make lithium-ion battery become the research hotspot. The estimation of parameters such as the charged state of lithium-ion batteries is very important for energy storage and management of lithium-ion batteries [2-4]. Accurate estimation of lithium-ion battery status

can make the management system more effective[5, 6]. Establishing a reasonable model to describe the characteristics of lithium-ion batteries is the premise of state estimation of lithium-ion batteries [7-11].

To describe the influencing factors and working characteristics of lithium-ion batteries intuitively, researchers engaged in lithium-ion battery research have established a variety of lithium-ion battery equivalent models.[12-18] The model can be divided into the electrochemical model, intelligent mathematical model, and the equivalent circuit model. The electrochemical model and intelligent mathematical model are relatively complex, and their application is limited by the high technical threshold. However, the equivalent circuit model is widely used because of its clear physical meaning and simple mathematical expression. There are four common equivalent physical models of lithium-ion batteries [19, 20]. (1) The internal resistance equivalent model is used, in which the ideal voltage source is introduced to represent the open-circuit voltage. The internal resistance R_0 and open-circuit voltage U_{OC} are all functions related to the state-of-charge levels. Only the positive and negative of the current need to be determined to judge the charge-discharge direction. (2) The resistance-capacitance equivalent model can be obtained by using a resistance-capacitance circuit that can effectively describe the surface effect of the circuit. The model consists of three resistors and two capacitors, in which Ca is the capacity of the battery and C_b is the small capacitance produced by the surface effect of the battery. (3) Thevenin equivalent model can be obtained by combining the Internal resistance model and the resistance-capacitance model analog circuit, which can take the effects of temperature and polarization into account. (4) The PNGV equivalent model is proposed to the battery test manual. Based on the Thevenin model, the circuit is connected to a series with the capacitor $C_{b.}$ R0 is internal resistance. R_p is polarization resistance and C_p is polarization capacitance. The load current is described by i(t). U_L is the terminal voltage. To estimate the charged state and health state of the lithium-ion battery, an equivalent model of lithium-ion battery is constructed first. First, select a model from the lithium-ion battery model, and then carry out relevant research.[21, 22] With the rapid development of new energy vehicles and the wide application market, higher requirements are put forward for the status estimation of the lithium-ion battery, which makes the study of the lithium-ion battery application model more important. The estimation of lithium-ion battery state by using existing models can no longer meet the requirements of computational accuracy. More and more researchers improve the estimation accuracy by constructing composite equivalent models and adopting filtering algorithms[23-28]. Wang, SL improved the accuracy of the estimates by using the composite equivalent model and the Unscented Kalman Filtering algorithm.[29] Along with the increasing deep learning, some researchers began to use data-driven modeling, by constructing a neural network[30], and then through the training can realize the estimate of the lithium-ion battery status, this method does not need to build the actual physical model, just need enough data to train the neural network[31-33]. With the development of big data and 5G, this method is likely to replace the traditional method in the near future[34, 35]. As for the current research, it is mainly based on the physical model of lithium-ion battery and its composite equivalent model. Therefore, the comparison and selection of models are of vital importance. The fitting effects of the same model can vary greatly under different working conditions, and different equivalent models should be selected for different batteries. Lithium-ion batteries carry out complex electrochemical reactions during charging and discharging[36]. The process is nonlinear and the environment will have a great influence on it, which makes the modeling of lithium-ion batteries more complex[24, 37, 38]. However, the

accurate estimation of SOC depends on whether the model used is accurate or not, and the model that accurately describes the lithium-ion battery will get twice the result with half the effort for the estimation of SOC.

The traditional PNGV model can't accurately describe the polarization effect of the lithium-ion battery. In this paper, the PNGV model and second-order RC model were fused to form an improved PNGV model. The traditional recursive least square algorithm has the phenomenon of data saturation[26], and the forgetting factor is added to solve this problem. The optimal choice of forgetting factor is discussed under different working conditions, and the EKF is used to accurately estimate the SOC[39-41].

2. MATHEMATICAL ANALYSIS

2.1. Improved equivalent modeling

The construction of a lithium-ion battery model is very important for the estimation of lithium-ion battery SOC. The estimation accuracy and computational complexity are largely related to the model.

In these papers[42, 43], a PNGV model of lithium-ion battery is built to describe the lithium-ion battery, as shown in Figure 1. In the PNGV model, C_b is used to describe the change of open-circuit voltage caused by the cumulative effect of current. R_1 is the ohmic resistance, R_{P1} is the polarization resistance, and C_{P1} is the polarization capacitance. The PNGV model of the lithium-ion battery well represents the cumulative effect of current during the discharge process of the lithium-ion battery, which makes the equivalent model of lithium battery more accurate. However, it failed to characterize the surface effect of lithium-ion batteries.

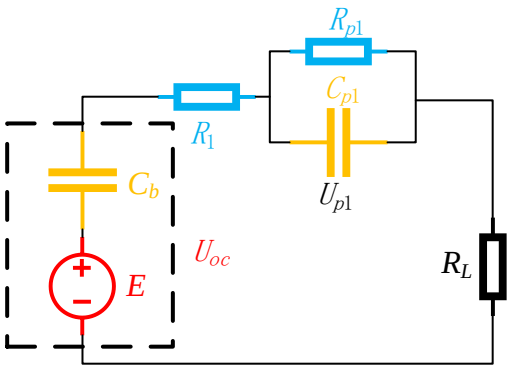

Figure 1. The PNGV model of lithium-ion battery

In these papers[19, 39], the second-order equivalent model is used to describe the lithium-ion battery, as shown in Figure 2.

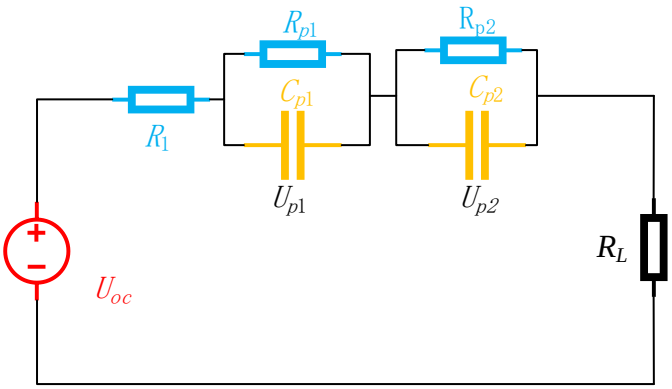

Figure 2. The second-order equivalent model of lithium-ion battery

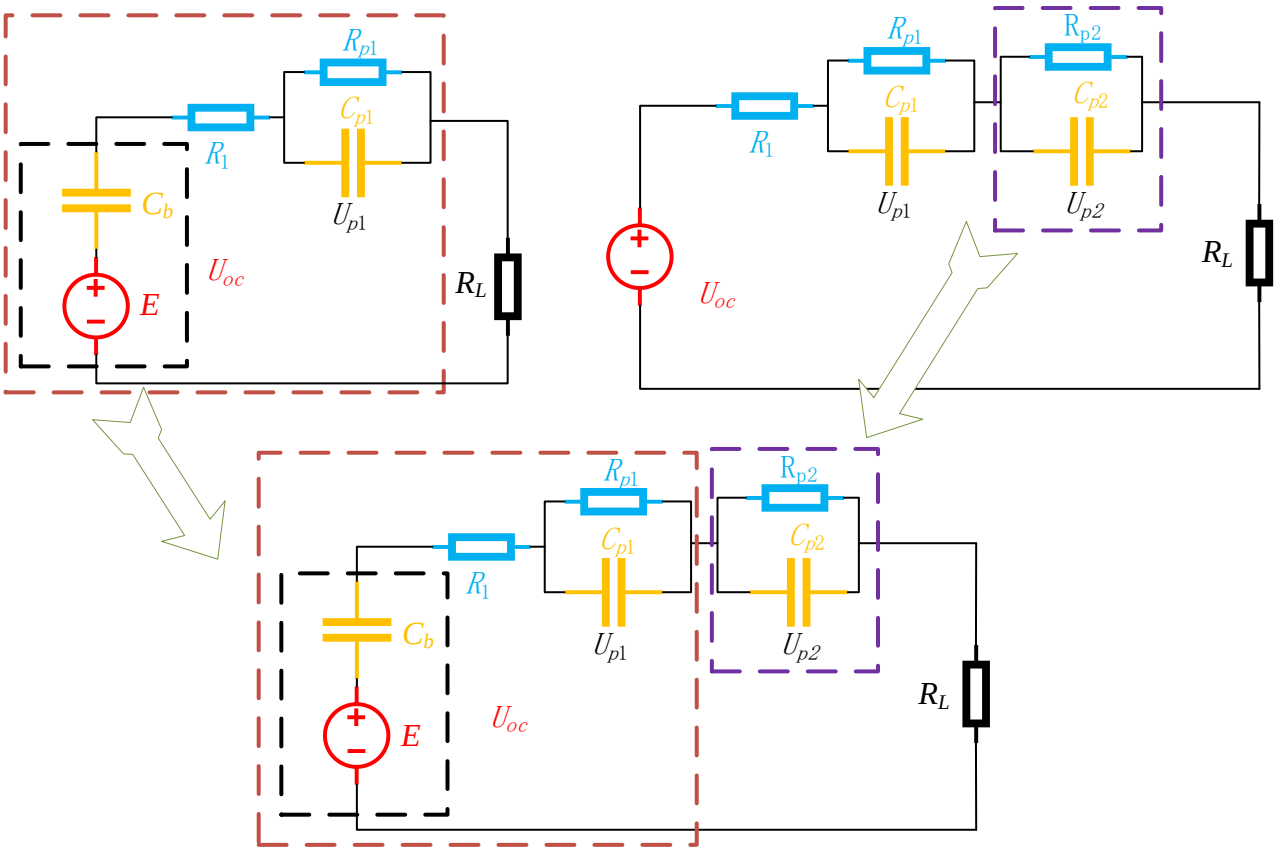

Figure 3. The improved PNGV model

In the second-order equivalent model, R_1 represents the ohmic resistance, R_{P1} represents the polarization resistance, C_{P1} represents the polarization capacitance, R_{P2} represents the surface effect resistance, and C_{p2} represents the surface effect capacitance. The second-order equivalent model of a lithium-ion battery cannot well represent the cumulative effect of current but has the advantage of characterizing the surface effect of a lithium-ion battery.

The PNGV model of lithium-ion batteries does not represent the surface effect of lithium-ion batteries, and the second-order equivalent model does not represent the cumulative effect of current

during the charge and discharge of lithium-ion batteries. In this paper, based on the PNGV model of the lithium-ion battery, an improved PNGV model was formed by combining the advantages of the second-order equivalent model of the lithium-ion battery. In the improved PNGV model, an RC loop is connected in series with the traditional PNGV model, which is used to simulate the surface effect resistance and surface effect capacitance of lithium-ion batteries, to accurately characterize the electrochemical reactions inside lithium-ion batteries. The improved PNGV model of lithium-ion batteries is shown in Figure 3.

In Figure 3, C_b is used to represent the change in the open-circuit voltage due to the cumulative effect of the current. U_{OC} stands for open-circuit voltage. U_l stands for terminal voltage. R_1 is ohmic internal resistance, U_{R1} is ohmic voltage, and is the effect of battery voltage drop at the moment of battery discharge and termination of discharge. The first *RC* parallel circuit is composed of polarization resistor R_{P1} and polarization capacitor C_{P1}, which is used to characterize the polarization effect of lithium battery, and U_{P1} is the polarization voltage. The second *RC* parallel circuit is composed of polarization resistor R_{P2} and polarization capacitor C_{p2}, which is used to characterize the surface effect of the lithium-ion battery, and U_{P2} is the surface effect voltage.

The calculation formula of capacitor C_b, which represents the current accumulation effect, is shown in Equation (1).

$$\Delta QU_{oc} = \frac{1}{2}\left[\left(U_{oc}+\Delta U_{oc}\right)^2 - U_{oc}^{\ 2}\right] \tag{1}$$

Capacitor C_b represents the amount of battery storage, and the simplified calculation formula of capacitor C_b can be obtained from the energy conservation law, as shown in Equation (2).

$$C_b = \frac{\Delta Q}{\Delta U_{oc}} \tag{2}$$

Where $\triangle Uoc$ represents the change of voltage within the calculated time, and $\triangle Q$ represents the change of electric quantity within the calculated time, which is measured by experiment.

According to Kirchhovsky's law, the established Thevenin equivalent circuit model is analyzed, and the voltage and current expressions of the equivalent circuit can be obtained as shown in Equation (3).

$$\begin{cases} U_L = U_{oc} - U_{R1} - U_{P1} - U_{P2} \\ I(t) = C_{P1}\dfrac{dU_{P1}}{dt} + \dfrac{U_1}{R_1} = C_{P2}\dfrac{dU_{P2}}{dt} + \dfrac{U_1}{R_1} \end{cases} \tag{3}$$

Among them, the open-circuit voltage U_{OC} is the stable voltage with the positive and negative ends of the battery in the static state for a long time, which can be obtained by the nonlinear function expression of SOC. By taking the parameters SOC, U_{P1}, U_{P2} to form the parameter matrix [SOC, U_{P1}, U_{P2}]$^{\mathrm{T}}$ as the state variable, the state space equation of lithium-ion battery is obtained through the above expression, as shown in Equations (4) and (5).

$$\begin{bmatrix} SOC(k+1) \\ U_{P1}(k+1) \\ U_{P2}(k+1) \end{bmatrix} = \begin{bmatrix} 1 & 0 & 0 \\ 0 & e^{-\frac{\Delta t}{R_{P1}C_{P1}}} & 0 \\ 0 & 0 & e^{-\frac{\Delta t}{R_{P2}C_{P2}}} \end{bmatrix} \times \begin{bmatrix} SOC(k) \\ U_{P1} \\ U_{P2} \end{bmatrix} + \begin{bmatrix} R_{P1}\left(1-e^{-\frac{\Delta t}{R_{P1}C_{P1}}}\right) \\ R_{P2}\left(1-e^{-\frac{\Delta t}{R_{P2}C_{P2}}}\right) \end{bmatrix} \left[I(t)\right] + \begin{bmatrix} \omega_{1,k} \\ \omega_{2,k} \end{bmatrix} \quad (4)$$

$$U_{L,k} = U_{oc,k} - R_{1,\ k} I_k - U_{C_b,k} + \begin{bmatrix} 0 \\ -1 \\ -1 \end{bmatrix}^T \begin{bmatrix} SOC_k \\ U_{P1,k} \\ U_{P2,k} \end{bmatrix} + \upsilon_k \quad (5)$$

Here Δt is the sampling interval, $\tau_1 = R_{P1} C_{P1}$, $\tau_2 = R_{P2} C_{P2}$. ω is the state error, υ is the measurement error, and is the zero-mean white noise of the covariance matrix ***Q*** and ***R***, respectively.

2.2. FMRLS online identification

The phenomenon of "data saturation" will appear in the traditional recursive least square algorithm with the increase in the number of iterations and the amount of data. The reason for this phenomenon is that the gain matrix will gradually approach zero with the increase of data quantity, which will result in the correction ability of the recursive least squares algorithm greatly reduced. Data saturation is a phenomenon in which more and more data are collected over time, and the information provided by the new data is covered by the old data. With the decline of the information provided by the new data, the self-correcting ability of system identification will gradually decrease. Because of this phenomenon, we need to reduce the influence of old data on system identification and increase the weight of newly acquired data in system identification. The commonly used methods to solve the phenomenon of data saturation include the fading memory method, the limited memory method, and the oscillating memory method. In this paper, the fading memory method is used to solve the problem of data saturation in the recursive least square algorithm. The least-square data fitting is to select a function fitting from a given function type according to a given data set, so as to minimize the sum of squares of residuals. As shown in Equation (6).

$$\begin{cases} \delta_i = y_i - y^*_i \\ \sum_{i=1}^{n} \delta_i^2 = \min\limits_{\varphi \in H} \sum_{i=1}^{n} \left[y_i - \varphi(x_i) \right]^2 \end{cases} \quad (6)$$

Where, y_i is the measured value at the current moment, and y^*_i is the data fitting value at the current moment. According to the improved PNGV model of the lithium-ion battery, the complex frequency domain equation can be obtained, as shown in Equation (7).

$$U_{OC}(s) - U_L(s) - U_{C_b}(s) = I(s) \frac{R_0 s^2 + \frac{1}{\tau_1 \tau_2}\left(R_0\tau_1 + R_0\tau_2 + R_{P1}\tau_2 + R_{P2}\tau_1\right)s + \frac{R_0 + R_{P1} + R_{P2}}{\tau_1 \tau_2}}{s^2 + \frac{(\tau_1 + \tau_2)s}{\tau_1 \tau_2} + \frac{1}{\tau_1 \tau_2}} \quad (7)$$

The transfer function in Equation (5) is discretized by bilinear transformation, and the discretized transfer function can be obtained, as shown in Equation (8).

$$G\left(Z^{-1}\right)=\frac{c_3+c_4Z^{-1}+c_5Z^{-2}}{1-c_1Z^{-1}-c_2Z^{-2}} \tag{8}$$

Where, C_1, C_2, C_3, C_4, and C_5 are the corresponding constant coefficients since the system is a single input single output system. Transform Equation (7) into a difference equation, as shown in Equation (9).

$$y(k+1)=U_{OC}-U_L-U_{C_b}=c_1y(k-1)+c_2y(k-2)+c_3I(k)+c_4I(k-1)+c_5I(k-2) \tag{9}$$

Where $I(k)$ is the system input and $y(k)$ is the system output. The relationship between lithium battery parameters and the constant coefficient can be deduced, as shown in Equation (10).

$$\begin{cases} R_1=\dfrac{c_3-c_4+c_5}{1+c_1-c_2} \\ \tau_1\tau_2=\dfrac{T^2\left(1+c_1-c_2\right)}{4\left(1-c_1-c_2\right)} \\ \tau_1+\tau_2=\dfrac{T\left(1+c_2\right)}{1-c_1-c_2} \\ R_1+R_{P1}+R_{P2}=\dfrac{c_3+c_4+c_5}{1-c_1-c_2} \\ R_1\tau_1+R_1\tau_2+R_{P1}\tau_2+R_{P2}\tau_1=\dfrac{T\left(c_3-c_5\right)}{1-c_1-c_2} \end{cases} \tag{10}$$

Input variables and parameter variable expressions are represented by matrices, as shown in Equation (11).

$$\begin{cases} \phi(k)=\left[y(k-1)\ y(k-2)\ I(k)\ I(k-1)\ I(k-2)\right] \\ \theta=\left[a_1\ a_2\ a_3\ a_4\ a_5\right] \end{cases} \tag{11}$$

The matrix expression of the system output can be obtained, as shown in Equation (12).

$$y(k)=\phi(k)^{\mathrm{T}}\theta+e(k) \tag{12}$$

On the basis of the recursive least square algorithm, the attenuation factor λ ($0<\lambda<1$) can be added to obtain the recursive formula (13) as follows

$$\begin{cases} \hat{\theta}(k+1)=P(k+1)\left[\lambda^2P(k)^{-1}\hat{\theta}(k)+\phi(k+1)y(k+1)\right] \\ \qquad\qquad =\hat{\theta}(k)+K(k+1)\left[y(k+1)-\phi^T(k+1)\hat{\theta}(k)\right] \\ K(k+1)=\dfrac{P(k)\phi(k+1)}{\lambda^2+\phi^T(k+1)P(k)\phi(k+1)} \\ P(k+1)=\dfrac{1}{\lambda^2}\left[I-\dfrac{P(k)\phi(k+1)\phi^T(k+1)}{\lambda^2+\phi^T(k+1)P(k)\phi(k+1)}\right] \end{cases} \tag{13}$$

λ^2 is replaced by ρ, $\rho=\lambda^2$（$0<\rho<1$）, and ρ is called the forgetting factor. Thus, the formula of the recursive least square algorithm of the fading memory method can be obtained, as shown in Equation (14).

$$\begin{cases} K(k+1)=P(k)\phi(k+1)\left[\rho+\phi^T(k+1)P(k)\phi(k+1)\right]^{-1} \\ \hat{\theta}(k+1)=\hat{\theta}(k)+K(k+1)\left[y(k+1)-\phi^T(k+1)\hat{\theta}(k)\right] \\ P(k+1)=\frac{1}{\rho}\left[I-K(k+1)\phi^T(k+1)\right]P(k) \end{cases} \quad (14)$$

Wherein $\hat{\theta}(k)$ is the solution of the quantity at time k, $\varphi(k)$ is the input matrix at time k, k (k+1) is the gain at time k+1, and $P(k)$ is the covariance at time k.

2.3. Extended Kalman filter algorithm

The extended Kalman filter algorithm is used to estimate the nonlinear system, the nonlinear state-space model is linearized, and then the basic Kalman filter algorithm is used to implement the nonlinear system. The partial derivatives of the equation of state and the observation equation are obtained, and the Taylor series expansion of the equation of state and the observation equation is obtained. The nonlinear mapping function is linearized, and the system matrix corresponding to the iterative calculation of the Kalman filter is obtained. The state-space equation of the nonlinear discrete system is shown in Equation (15).

$$\begin{cases} x_{k+1} = f\left(X_k, k\right) + \omega_k = A_k x_k + B_k u_k + \omega_k \\ y_k = h\left(X_k, k\right) + \upsilon_k = C_k x_k + D_k + \upsilon_k \end{cases} \quad (15)$$

Where X_k is the state variable and U_K is the system input. y_k is the observation variable, A_k is the state transition matrix, which is used to predict the system variables, B_k is the system control input matrix, C_k and D_k are the system observation matrix, which drives and predicts the system observation quantity. ω_k and υ_k are stating error and observation error respectively. According to Equations (4) and (5), the expressions of A_k, B_k, C_k and D_k can be obtained, as shown in Equation (16).

$$\begin{cases} A_k = \dfrac{\partial f(x_k, k)}{\partial x_k}\Big|_{x_k=\hat{x}_k} \\ B_k = f(\hat{x}_k, k) - A_k\hat{x}_k \\ C_k = \dfrac{\partial h(x_k, k)}{\partial x_k}\Big|_{x_k=\hat{x}_k} \\ D_k = h\left(\overline{X_k}, k\right) - C_k\overline{X_k} \end{cases} \quad (16)$$

The recursive process formula of the extended Kalman filter algorithm is shown in Equation (17).

$$\begin{cases} \overline{X_{k+1}^{-}} = f\left(X_k\right) \\ \overline{P_{k+1}^{-}} = A_k \overline{P_k} A_k^T + Q_{k+1} \\ K_{k+1} = \overline{P_{k+1}^{-}} C_{k+1}^T \left(C_{k+1} \overline{P_{k+1}^{-}} C_{k+1}^T + R_{k+1}\right)^{-1} \\ \overline{X_{k+1}} = X_{k+1}^{-} + K_{k+1}\left[Z_{k+1} - h\left(X_{k+1}^{-}\right)\right] \\ \overline{P_{k+1}} = \left[I + K_{k+1} C_{k+1}\right] P_{k+1}^{-} \end{cases} \tag{17}$$

Where ***P*** is the mean square error and ***K*** is the Kalman gain. ***I*** is the identity matrix. ***Q*** and ***R*** are the variances of ω and υ, respectively.

2.4 Algorithm evaluation criteria

To evaluate the advantages and disadvantages of the estimation method, the estimated SOC results are compared with the actual results. Since the obtained data are obtained on the test instrument, the measurement accuracy is relatively high. Here, the SOC value obtained by the ampere-hour integration method is taken as the true value. On this basis, three statistics of mean absolute error (MAE), mean absolute percentage error (MAPE) and root mean square error (RMSE) were selected as the evaluation criteria. The calculation formula of these three evaluation errors is shown in Equation (18).

$$\begin{cases} MAE = \dfrac{1}{N}\sum_{i=1}^{N}\left|Y_i - \overline{Y_i}\right| \\ MAPE = \dfrac{1}{N}\sum_{i=1}^{N}\left|\dfrac{Y_i - \overline{Y_i}}{Y_i}\right| * 100\% \\ RMSE = \sqrt{\dfrac{1}{N}\sum_{i=1}^{N}\left(Y_i - \overline{Y_i}\right)^2} \end{cases} \tag{18}$$

In the calculation formula, Y_i represents the real value of the SOC at i time. $\ddot{Y}_i$ represents the estimated value of the SOC at i time; N is the total number of estimates.

3. EXPERIMENTAL ANALYSIS

3.1. Test platform construction

The experiment takes ternary power lithium-ion battery as the object, its rated capacity is 70Ah, charging cut-off voltage is 4.20V, discharging cut-off voltage is 2.75V. Battery experimental charging and discharging equipment is the power battery large-rate charge and discharge tester (BTS-750-200-100-4) of Shenzhen Yakeyuan Technology Co. LTD, with the maximum charging and discharging power of 750W, the maximum current of 100A, and the maximum voltage of 200V. The basic technical parameters are shown in Table.1.

Table 1. Basic technical parameters of the battery

Factor	parameter
Size: length * width * height /mm	200*80*180
Rated voltage/V	3.65
Maximum load current /A	1.5C
Charge cut-off voltage/V	4.2
Discharge cutoff voltage/V	2.75
Working temperature /℃	-15~70
Rated capacity/Ah	70.0

3.2. Hybrid pulse power characterization Test (HPPC) experiment

HPPC Test is a Battery performance Test method proposed in the 《FreedomCAR Battery Test Manual For Power-Assist Hybrid Electric Vehicles》. Through the HPPC test, the model parameters can be effectively identified[29, 44].

To obtain the required change rule of the closed-circuit voltage output response of the lithium-ion battery pack, the lithium-ion battery is first charged through constant current and constant voltage charging. At this time, the charged state of the battery is full, that is, the SOC value is 100%. After a period of standing, the internal chemical state tends to be stable and the HPPC experiment is started. During the experiment, discharge was carried out through the intermittent cycle of 1C discharge current. In the test process, the 1CA intermittent cycle discharge process was used for discharge and HPPC experimental analysis was carried out in combination with the use link. During the process, the battery is discharged for 10s and left to rest for 40s, charged for 10s, left to rest for 5 minutes, discharged for 6 minutes and then left to rest for 40 minutes. This process is continued for the discharge cycle experiment until the SOC reaches 0.000%. The current and voltage variations of lithium-ion batteries were recorded during the experiment. The cycle is shown in Figure.4. In the figure, the discharge is performed at an interval of 40 minutes, and an HPPC test is unrolled at the end of the set of 40 minutes. The HPPC test embedded during the intermittent discharge is performed at the shelf-end shown in the figure, and the current pulse, which lasts for 10 seconds at the end of each shelf-time, is expanded at the end of the shelf-time. Aiming at the parameter identification problem of the constructed Thevenin model and its state-space equation, 1CA constant current pulse charging-discharging experiment was carried out at room temperature based on the HPPC method of mixed pulse power characteristic test. Through the pulse charging and discharging process and the analysis of the working principle of the battery pack, the correlation between various model parameters or other parameters is obtained.

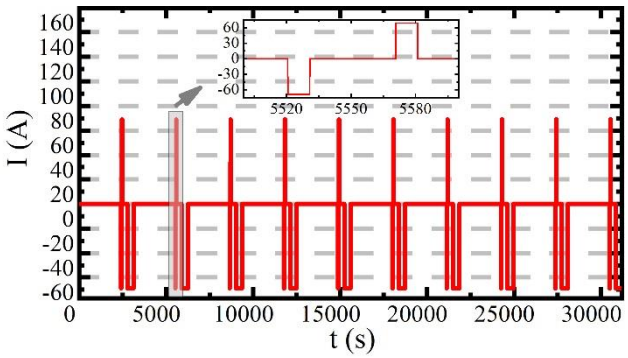

Figure 4. Intermittent discharge process

Based on the experimental analysis, considering the influence of different SOC values on the difference between charge and discharge, the dynamic working characteristics of the lithium-ion battery pack are obtained and used for the identification of various parameters in the equivalent model. The experimental process of designing HPPC is shown in Figure.5.

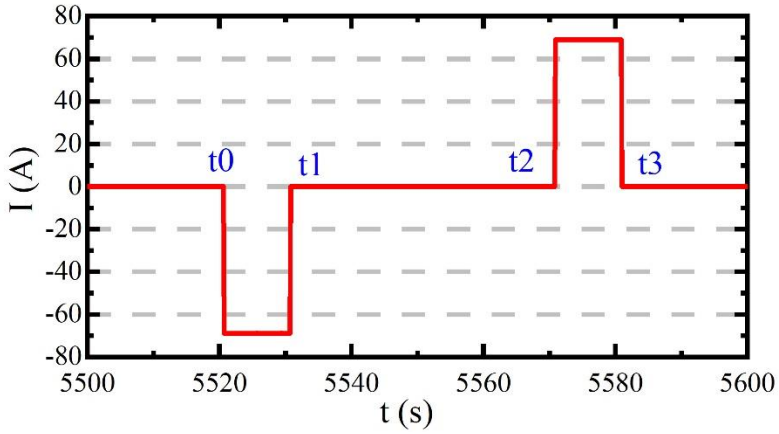

Figure 5. HPPC test procedure

According to the analysis, the experimental steps of a single HPPC test are as follows:

Step 1: Perform 1CA multiplier constant current pulse discharge for 10s, as shown in the figure from t0 to t1.

Step 2: Let go of the 40s, as shown in figure t1 to t2.

Step 3: Perform constant current 1C pulse charging for 10s, as shown in the time period t2 to t3 in the figure.

Step 4: Set aside 40s.

During the whole parameter identification experiment, HPPC tests were carried out for SOC values at different moments at the same time interval.

S1: The lithium-ion battery is charged to full capacity by charging at constant voltage with constant current first. In the phased process, constant current fast charging was used respectively, and

then the constant pressure supplementing mode was changed to make its SOC value 100%. After standing for 40 minutes, HPPC was tested and the process data was recorded.

S2: Conduct constant current discharge on the battery pack and release 10% of the power to reduce its SOC value to 90%, and conduct HPPC test under the condition of this SOC value.

S3: And so on, 100%, 90%, 80%, …, 20%, 10%, and 0% of the HPPC test, and then the model parameters under different SOC conditions were obtained for the subsequent parameter identification process.

Assuming that the parameter U_{OC} remains stable during this short duration, the battery pack's corresponding closed-circuit voltage response is recorded with each current pulse. The cyclic current pulse was repeated at every 10%SOC drop until the li-ion battery was discharged completely. The closed-circuit voltage response is obtained by embedded current pulse under these SOC conditions and then used for parameter identification. The coefficients of the function equation are obtained by the battery's closed-circuit voltage response combined with its embedded current pulses.

3.3. Dynamic stress test (DST) experiment

DST experiment of lithium battery is a kind of complex operating condition of lithium battery, which can verify the practicability and robustness of the algorithm to the greatest extent[45, 46]. The experimental steps of lithium battery DST experimental conditions are shown in Table.2.

Table 2. Parameters and descriptions of DST

Step	Complete steps(t/s)	Add up(t/s)	Percentage of the maximum power of the vehicle
1	16	16	0%
2	28	44	-13%
3	12	56	-25%
4	8	64	13%
5	16	80	-2%
6	24	104	-13%
7	12	116	-25%
8	8	124	13%
9	16	140	-2%
10	24	164	-13%
11	12	176	-25%
12	8	184	25%
13	16	200	-2%
14	36	236	-13%
15	2	238	-100%
16	6	244	-50%
17	24	268	-63%
18	8	276	25%
19	32	308	-25%

20	8	316	50%
21	12	328	-2%
22	2	330	-121%
23	5	335	-2%
24	2	337	66%
25	23	360	-2%

The running time and cumulative time of each working step are given in the experimental working step table. In the experiment, the capacity of the selected battery was taken as the capacity of the whole vehicle. The percentage of discharge capacity is taken as a percentage of the total capacity of the battery.

3.4. Beijing bus dynamic stress test (BBDST) experiment

The battery voltage, current, and speed of a line of pure electric buses in Beijing were measured. The operating conditions of BBDST are calculated as shown in Table.3.

Table 3. Parameters and descriptions of BBDST

Step	P/kW		t/s		State description
	Open-air conditioning	Close air conditioning	Complete steps	Add up	
1	45	37.5	21	21	Start
2	80	72.5	12	33	Accelerate
3	12	4.5	16	49	Taxiing
4	-15	-15.0	6	55	Braking
5	45	37.5	21	76	Accelerate
6	12	4.5	16	92	Taxiing
7	-15	-15.0	6	98	Braking
8	80	72.5	9	107	Accelerate
9	100	92.5	6	113	Rapidly accelerate
10	45	37.5	21	134	Constant speed
11	12	4.5	16	150	Taxiing
12	-15	-15.0	6	156	Braking
13	80	72.5	9	165	Accelerate
14	100	92.5	6	171	Rapidly accelerate
15	45	37.5	21	192	Constant speed
16	12	4.5	16	208	Taxiing
17	-35	-35.0	9	217	Braking
18	-15	-15.0	12	229	Braking
19	12	4.5	71	300	End

The running time and cumulative time of each working step are given in the experimental working step table. The running state of the electric vehicle corresponding to each work step can also be seen in the table. In the experiment, the discharge power of the lithium-ion battery in each working step is divided into two conditions: air conditioning on and air conditioning off. When setting up the

experiment, one of the two conditions can be randomly selected to conduct the experiment.

3.5. Parameter identification results

The BTS200-100-104 battery detection equipment produced by Shenzhen Yakeyuan Technology Co., Ltd. was used as the experimental platform to obtain real-time operation data of the lithium-ion batteries. The recursive least square method with fading memory was used to identify the relevant parameters of the improved PNGV model of lithium-ion battery online, and the identification results were shown in Figure 6.

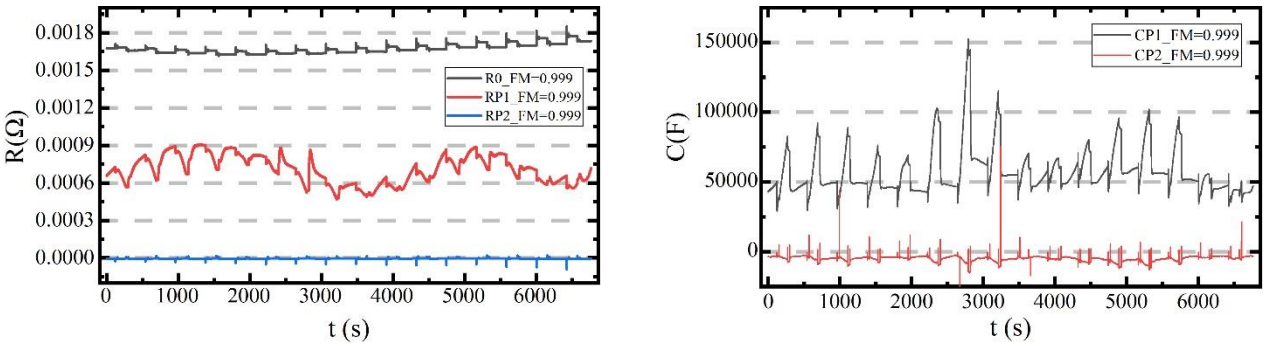

a. on-line identification resistance b. on-line identification capacitance

Figure 6. PNGV model fitting result

In the beginning, the value of capacitor C_b can be calculated through Equation (2), as shown in Equation (19).

$$C_b = \frac{\Delta Q}{\Delta U_{oc}} = \frac{68.4771*10}{68.47714.1821\text{-}4.175} = 96466.61972\ (\text{F}) \tag{20}$$

3.6. Analysis of experimental results

The actual calibration capacity of the lithium-ion battery selected for the experiment was 68.4771Ah, and the BTS200-100-104 battery detection equipment provided by Shenzhen Yakeyuan Co., Ltd was used as the experimental platform to collect the experimental data in real-time. Two different conditions of the lithium-ion battery were used respectively. The experiment uses the SOC value obtained by the AH integration method as the accurate value and discusses the optimal SOC value accurately estimated by the forgetting factor recursive least square method under the two working conditions.

DST is the test condition of the lithium-ion battery. In this condition, the estimation accuracy of lithium-ion battery SOC under different forgetting factors is analyzed and compared. By comparing the three evaluation criteria of absolute error, mean absolute percentage error and root mean square error under different forgetting factors, it can be concluded that the estimation accuracy of the selected

lithium-ion battery is the most accurate when the forgetting factor is 0.999. The three evaluation criteria under different forgetting factors are shown in Figure 7.

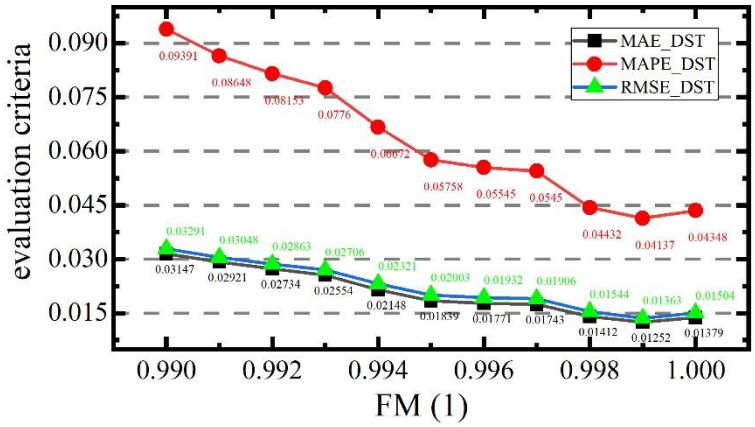

Figure 7. Error under DST condition in different Fading Memory

It can be seen from the figure that the estimation accuracy of the SOC of the lithium-ion battery is continuously improved with the increasing forgetting factor. When the forgetting factor is 0.999, the three evaluation errors all reach the minimum value, that is, the estimation result of the SOC at this time is the most accurate. The estimation results obtained by the proposed online estimation algorithm are shown in Figure 8.

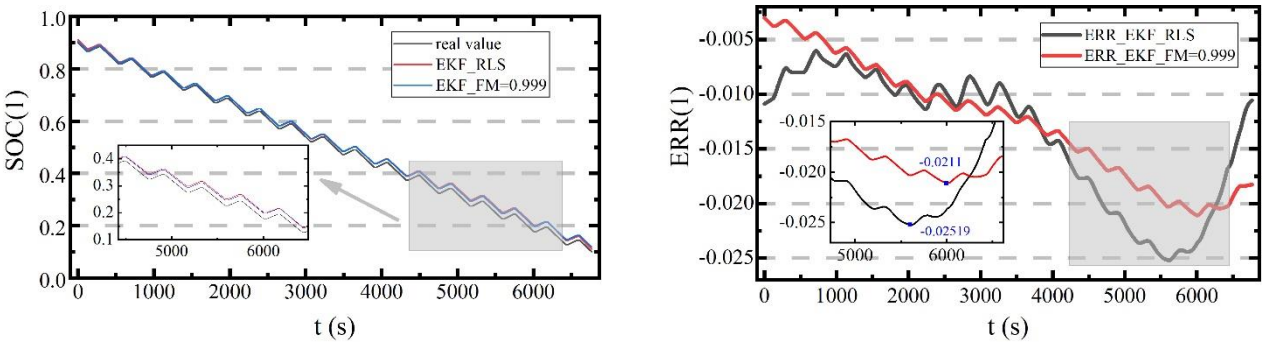

a. estimation under DST condition b. estimation Error under DST condition

Figure 8. SOC estimation results under DST condition

It can be seen from the figure that the maximum error of the recursive least square method of fading memory for SOC estimation under DST condition is -2.11%. The average absolute error is 0.01252, the average absolute percentage error is 0.04137, the average absolute percentage error is 4.85%, and the root means square error is 0.01363, the relative recursive least square method is 9.38%. Compared with [47-49], the accuracy and convergence of SOC estimation are improved.

BBDST is a kind of actual power lithium-ion battery operating condition in Beijing bus operation. The selection of this kind of operating condition has practical guiding significance for the actual accurate estimation of lithium-ion battery SOC. By comparing the three evaluation criteria of absolute error, mean absolute percentage error and root mean square error under different forgetting factors, it can be concluded that the estimation accuracy of the selected lithium-ion battery is the most accurate when the forgetting factor is 0.993. The three evaluation criteria under different forgetting factors are shown in Figure 9.

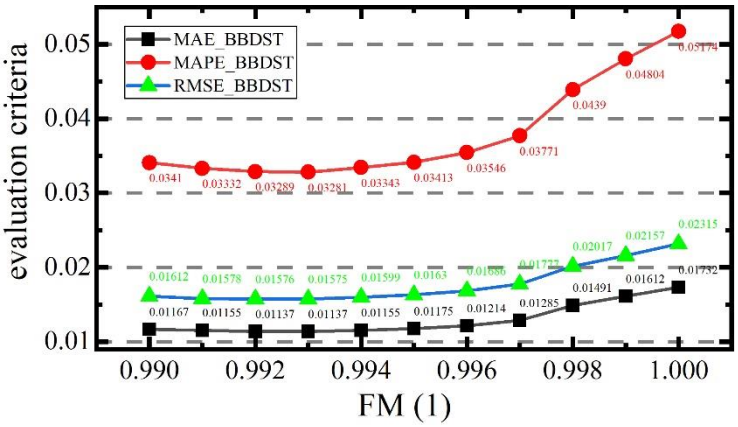

Figure 9. Error under BBDST condition in different Fading Memory

As can be seen from the figure, as the forgetting factor increases, the estimation accuracy of the SOC of the lithium-ion battery first increases and then decreases. When the forgetting factor is 0.993, the three evaluation errors all reach the minimum value, that is, the estimation result of the SOC at this time is the most accurate. The estimation results obtained by the proposed online estimation algorithm are shown in Figure 10.

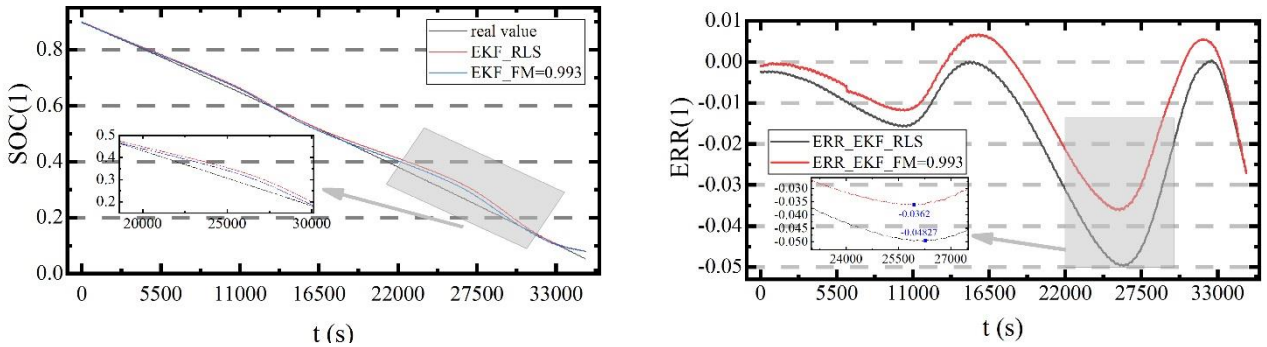

a. estimation under BBDST condition b. estimation Error under BBDST condition

Figure 10. SOC estimation results under BBDST condition

It can be seen from the figure that the maximum error of SOC estimation by recursive least square method of fading memory under BBDST condition is -3.62%. The average absolute error of 0.01137

improves the estimation accuracy by 34.35%, the average absolute percentage error of 0.03281 improves the estimation accuracy by 36.59% and the root means a square error of 0.01575 improves the estimation accuracy by 31.97%. Compared with [47, 50, 51], the accuracy and convergence of SOC estimation are improved.

4. CONCLUSIONS

In this paper, the PNGV model and the recursive least squares algorithm of the lithium-ion battery are improved. On this basis, an accurate estimation algorithm of lithium-ion battery SOC is proposed based on FMRLS and an improved PNGV model. The proposed algorithm effectively improves the SOC estimation accuracy of lithium-ion batteries. The estimation accuracy of MAE, MAPE, and RMSE improves by 9.21%, 4.85%, and 9.38%, respectively, under DST condition, and by 34.35%, 36.59%, and 31.97%, respectively, under BBDST condition. It has a very high reference value for the actual estimation of electric vehicle SOC.

ACKNOWLEDGMENTS
The work was supported by National Natural Science Foundation of China (No. 61801407) and Natural Science Foundation of Southwest University of Science and Technology (No. 17zx7110)

References

1. L. Sun, G. Li and F. You, *Renewable & Sustainable Energy Reviews*, 131 (2020) 892.
2. F. Xiao, C. Li, Y. Fan, G. Yang and X. Tang, *International Journal of Electrical Power & Energy Systems*, 124 (2021) 728.
3. C. Yang, X. Wang, Q. Fang, H. Dai, Y. Cao and X. Wei, *Journal of Energy Storage*, 29 (2020) 954.
4. Y. C. Fan, S. L. Wang, C. Jiang and C. Fernandez, *Int. J. Electrochem. Sci.*, 16 (2021) 28.
5. Z. Q. Lyu and R. J. Gao, *Int J Energ Res*, 44 (2020) 10262.
6. M. S. H. Lipu, M. A. Hannan, T. F. Karim, A. Hussain, M. H. M. Saad, A. Ayob, M. S. Miah and T. M. I. Mahlia, *J Clean Prod*, 292 (2021) 27.
7. Z. G. Chen, J. X. Zhou, F. Zhou and S. Xu, *J Clean Prod*, 290 (2021) 534.
8. S. Q. Li, C. K. Ju, J. L. Li, R. Fang, Z. F. Tao, B. Li and T. T. Zhang, *Energies*, 14 (2021) 249.
9. X. Y. Li, Z. J. Huang, J. D. Tian and Y. Tian, *Energy*, 220 (2021) 89.
10. Y. F. Liu, J. Q. Li, G. Zhang, B. Hua and N. Xiong, *Ieee Access*, 9 (2021) 34177.
11. D. M. Sun, X. L. Yu, C. M. Wang, C. Zhang, R. Huang, Q. Zhou, T. Amietszajew and R. Bhagat, *Energy*, 214 (2021) 228.
12. Y.-j. Ji, S.-l. Qiu and G. Li, *Journal of Central South University*, 27 (2020) 2606.
13. K. Saleem, K. Mehran and Z. Ali, *Electric Power Systems Research*, 185 (2020) 572.
14. S. Wang, C. Fernandez, C. Yu, Y. Fan, W. Cao and D.-I. Stroe, *Journal of Power Sources*, 471 (2020) 764.
15. T. Zhao, Y. Zheng, J. Liu, X. Zhou, Z. Chu and X. Han, *International Journal of Energy Research*, (2020) 543.
16. F. Guo, G. Hu, P. Zhou, T. Huang, X. Chen, M. Ye and J. He, *International Journal of Energy Research*, 43 (2019) 9013.
17. H. Ren, Y. Zhao, S. Chen and L. Yang, *International Journal of Energy Research*, 43 (2019) 7306.
18. J. Sihvo, T. Roinila and D. I. Stroe, *IEEE Trans. Ind. Electron.*, 68 (2021) 4916.

19. Y. Y. Fang, Q. Zhang, H. Zhang, W. C. Xu, L. S. Wang, X. L. Shen, F. L. Yun, Y. Cui, L. Wang and X. Zhang, *IET Power Electron.*, 14 (2021) 38.
20. Y. Gao, R. J. Huang, D. C. Qin, T. T. Wang, S. B. Ma and S. Qin, *Int. J. Electrochem. Sci.*, 16 (2021) 27.
21. L. Jiang, Y. Li, J. Ma, Y. Cao, C. Huang, Y. Xu, H. Chen and Y. Huang, *Renewable Energy*, 160 (2020) 1385.
22. H. Ren, H. Zhang, Z. Gao and Y. Zhao, *Journal of Cleaner Production*, 270 (2020) 1045.
23. X. B. Chen, X. P. Chen and X. W. Chen, *Int J Energ Res*, (2021) 276.
24. Y. He, Q. Li, X. X. Zheng and X. T. Liu, *J Power Electron*, 21 (2021) 590.
25. D. Y. Huang, Z. Q. Chen and S. Y. Zhou, *Energy*, 216 (2021) 751.
26. X. L. Liu, Y. Jin, S. Zeng, X. Chen, Y. Feng, S. Q. Liu and H. L. Liu, *Csee J Power Energy*, 6 (2020) 735.
27. N. Tian, H. Z. Fang, J. Chen and Y. B. Wang, *Ieee T Contr Syst T*, 29 (2021) 370.
28. S. Z. Zhang, X. Guo and X. W. Zhang, *J Energy Storage*, 33 (2021) 843.
29. S. L. Wang, C. Fernandez, C. M. Yu, Y. C. Fan, W. Cao and D. I. Stroe, *J. Power Sources*, 471 (2020) 13.
30. L. Ma, C. Hu and F. Cheng, *J Energy Storage*, 37 (2021) 731.
31. M. A. Hannan, D. N. T. How, M. S. H. Lipu, P. J. Ker, Z. Y. Dong, M. Mansur and F. Blaabjerg, *IEEE Trans. Power Electron.*, 36 (2021) 7349.
32. J. P. Tian, R. Xiong, W. X. Shen and J. H. Lu, *Appl. Energy*, 291 (2021) 10.
33. D. Burzynski and L. Kasprzyk, *Knowledge-Based Syst.*, 219 (2021) 11.
34. K. L. Liu, Y. L. Shang, Q. Ouyang and W. D. Widanage, *IEEE Trans. Ind. Electron.*, 68 (2021) 3170.
35. Y. J. Guo, Z. L. Yang, K. L. Liu, Y. H. Zhang and W. Feng, *Energy*, 219 (2021) 13.
36. Z. Ren, C. Q. Du, Z. Y. Wu, J. B. Shao and W. J. Deng, *Int J Energ Res*, 20 (2021) 137.
37. D. M. Sun, X. L. Yu, C. M. Wang, C. Zhang, R. Huang, Q. Zhou, T. Amietszajew and R. Bhagat, *Energy*, 214 (2021) 14.
38. D. Y. Huang, Z. Q. Chen and S. Y. Zhou, *Energy*, 216 (2021) 15.
39. Z. Y. Zhang, L. Jiang, L. Z. Zhang and C. X. Huang, *J Energy Storage*, 37 (2021) 15.
40. Y. C. Fan, H. T. Shi, S. L. Wang, C. Fernandez, W. Cao and J. H. Huang, *Energies*, 14 (2021) 18.
41. Z. J. Huang, Y. S. Fang and J. J. Xu, *Int. J. Automot. Technol.*, 22 (2021) 335.
42. X. Y. Liu, W. L. Li and A. G. Zhou, *Ieee Access*, 6 (2018) 23639.
43. K. J. Pai, *Electronics-Switz*, 8 (2019) 84.
44. H. B. Jiang, X. J. Chen, Y. F. Liu, Q. Zhao, H. H. Li and B. Chen, *Energies*, 14 (2021) 19.
45. X. D. Sun, J. R. Ji, B. Y. Ren, C. X. Xie and D. Yan, *Energies*, 12 (2019) 15.
46. C. X. Yu, Y. M. Xie, Z. Y. Sang, S. Y. Yang and R. Huang, *Energies*, 12 (2019) 19.
47. M. Fasahat and M. Manthouri, *J. Power Sources*, 469 (2020) 8.
48. L. L. Li, Z. F. Liu and C. H. Wang, *J. Test. Eval.*, 48 (2020) 1712.
49. C. F. Yang, X. Y. Wang, Q. H. Fang, H. F. Dai, Y. Q. Cao and X. Z. Wei, *J Energy Storage*, 29 (2020) 14.
50. Y. Kawahara, K. Sakabe, R. Nakao, K. Tsuru, K. Okawa, Y. Aoshima, A. Kudo and A. Emori, *J. Power Sources*, 481 (2021) 6.
51. W. Xiaogang, X. Li, N. I. Shurov, A. A. Shtang, M. V. Yaroslavtsev and S. I. Dedov, *Journal of Siberian Federal University. Engineering and Technologies*, 13 (2020) 420.